

# The universally growing mode in the solar atmosphere: coronal heating by drift waves

J. Vranjes<sup>\*</sup> and S. Poedts<sup>†</sup>

*K. U. Leuven, Center for Plasma Astrophysics, Celestijnenlaan 200B, 3001 Leuven, Belgium,  
and Leuven Mathematical Modeling and Computational Science Center (LMCC)*

Accepted xxx. Received xxx; in original form xxx

## ABSTRACT

The heating of the plasma in the solar atmosphere is discussed within both frameworks of fluid and kinetic drift wave theory. We show that the basic ingredient necessary for the heating is the presence of density gradients in the direction perpendicular to the magnetic field vector. Such density gradients are a source of free energy for the excitation of drift waves. We use only well established basic theory, verified experimentally in laboratory plasmas. Two mechanisms of the energy exchange and heating are shown to take place simultaneously: one due to the Landau effect in the direction parallel to the magnetic field, and another one, stochastic heating, in the perpendicular direction. The stochastic heating i) is due to the electrostatic nature of the waves, ii) is more effective on ions than on electrons, iii) acts predominantly in the perpendicular direction, iv) heats heavy ions more efficiently than lighter ions, and v) may easily provide a drift wave heating rate that is orders of magnitude above the value that is presently believed to be sufficient for the coronal heating, i.e.,  $\simeq 6 \cdot 10^{-5}$  J/(m<sup>3</sup>s) for active regions and  $\simeq 8 \cdot 10^{-6}$  J/(m<sup>3</sup>s) for coronal holes. This heating acts naturally through well known effects that are, however, beyond the current standard models and theories.

**Key words:** Sun: corona, oscillations.

## 1 INTRODUCTION

The physical parameters in all three main regions of the solar atmosphere (photosphere, chromosphere and corona) change both horizontally and with altitude. This by all means also includes the collisional frequency, with respect to which the solar atmosphere could be, roughly speaking, termed as ‘strongly collisional’ (in the photosphere and in the lower part of the chromosphere), ‘mildly collisional’ (in the upper part of the chromosphere), and ‘collision-less’ (in most of the corona and beyond). This classification is not absolute as it depends on the ratio of the characteristic time  $\tau_c$  for certain physical process, and the collisional time  $\tau_\nu \sim 1/\nu$ , where  $\nu$  is the collision frequency. The collisions of plasma species include those between plasma particles (e-i, e-e, i-i), i.e., Coulomb type collisions (which are typical for the corona), and those between plasma particles and un-ionized neutrals, e-n and i-n (which are absolutely dominant in the photosphere and in the lower part of the chromosphere). In the photosphere, for example, the ion-neutral and electron-neutral collision frequencies (Vranjes et al. 2007,

2008a; Pandey & Wardle 2008) are about  $10^9$  and  $10^{10}$  Hz, respectively, while the ion-ion and electron-ion Coulomb collision frequencies are around  $10^7$  and  $10^9$  Hz, respectively. In the corona, the Coulomb collisions occur much less frequent:  $\nu_{ei} \simeq 36$  Hz and  $\nu_{ii} \simeq 1$  Hz (for  $n_0 = 10^{15}$  m<sup>-3</sup>), and  $\nu_{ei} \simeq 0.4$  Hz and  $\nu_{ii} \simeq 0.01$  Hz (for  $n_0 = 10^{13}$  m<sup>-3</sup>).

All plasma modes (with probably one exception only, see below) are generally damped by collisions, and therefore a strong source is needed whenever one deals with waves in the (lower) solar atmosphere. However, such a (local!) source sustaining the waves over longer distances or time intervals is most often absent, even in models for coronal heating by waves. On the other hand, in the practically collision-less and very hot corona, Landau damping occurs and damps plasma waves very effectively by hot resonant ions, so that in this region too, a wave source is required to sustain the waves over a longer time interval.

There is only one mode that is able to survive the drastically different (collisional-collisionless) extremes in the different layers of the solar atmosphere, viz. *the drift mode*. Moreover, this mode is able to benefit (grow) from each of these extreme situations. This drift mode has been called the ‘universally growing mode’ in the literature. In collisional plasma, the drift mode grows due to the electron collisions

<sup>\*</sup> E-mail: Jovo.Vranjes@wis.kuleuven.be; jvranjes@yahoo.com

<sup>†</sup> E-mail: Stefaan.Poedts@wis.kuleuven.be

and this can be described within the two-fluid model. In collision-less plasma, however, the mode grows due to the electron resonance effect in the presence of a density gradient, but this is a purely kinetic effect. The fluid description works very well in the lower solar atmosphere, simply due to the fact that the plasma is so strongly collisional there (i.e., the Maxwellization is very effective). On the other hand, the kinetic description is preferred in the collision-less environment in the corona. Hence, in both extremes we have a proper environment and a proper theoretical model for studying the strong instabilities of the drift waves. Nevertheless, the driving mechanism for the waves is the same in both cases, namely *the presence of a density gradient* perpendicular to the ambient magnetic field vector.

Numerous observations confirm the presence of such density irregularities. Yet, the impression is that the possible role of the drift wave in the coronal heating problem is either overlooked or strongly underestimated (the mode is never mentioned in any book dealing with solar plasma). This may be partly due to the fact that the drift wave necessarily implies a multi-component fluid or kinetic description, contrary to the widely used single-fluid magnetohydrodynamics (MHD) model, within which the drift wave simply can not be studied.

The heating of the corona is one of the long-standing puzzles in solar physics and relates to the question of why the temperature of the Sun's corona is about  $1$  to  $3 \times 10^6$  K (parts of the corona are even hotter) while the solar surface is only around  $5600$  K hot. A detailed review of the problem may be found in Narain & Umschneider (1990); Klimtchuk (2006). According to Narain & Umschneider (1990) the necessary heating rates for active regions and coronal holes are around  $6 \cdot 10^{-5}$  J/(m<sup>3</sup>s) and  $8 \cdot 10^{-6}$  J/(m<sup>3</sup>s), respectively. Similar values and a detailed analysis of the problem may be found also in Aschwanden (2004). Two theories on coronal heating, namely wave heating [e.g. Suzuki (2004)] and magnetic reconnection (or nanoflares), have remained as the most likely candidates, and many solar physicists believe that some combination of these two theories can probably explain coronal heating, although 'the details are not yet complete'. Both models, however, rely on the continuum approximation (MHD) while it is clear that the actual heating takes place at length scales much smaller than those on which the MHD model is justified. Moreover, it is evident that the observed discrepancy between the ion and electron temperatures in the corona as well as the observed large temperature anisotropy, with a proton perpendicular temperature higher than the parallel temperature, are beyond the (single!) fluid model. Note also that according to a recent study (Regnier et al. 2008), the distribution of magnetic null points (only 2% of them are located in the corona and 54% in the photosphere) is opposite to what would be required for the mechanism that is supposed to heat the corona. The heating by waves rather than by reconnection is also supported by the diagnostic of active regions presented in Milligan et al. (2005).

A self-consistent heating model must fulfil a lot of requirements. It must: 1) provide an energy source for the extremely high temperature in corona, including 2) a reliable and efficient mechanism for the energy transfer from the source to the plasma particles, and 3) this with a required heating rate. It should also 4) explain the discrepancy be-

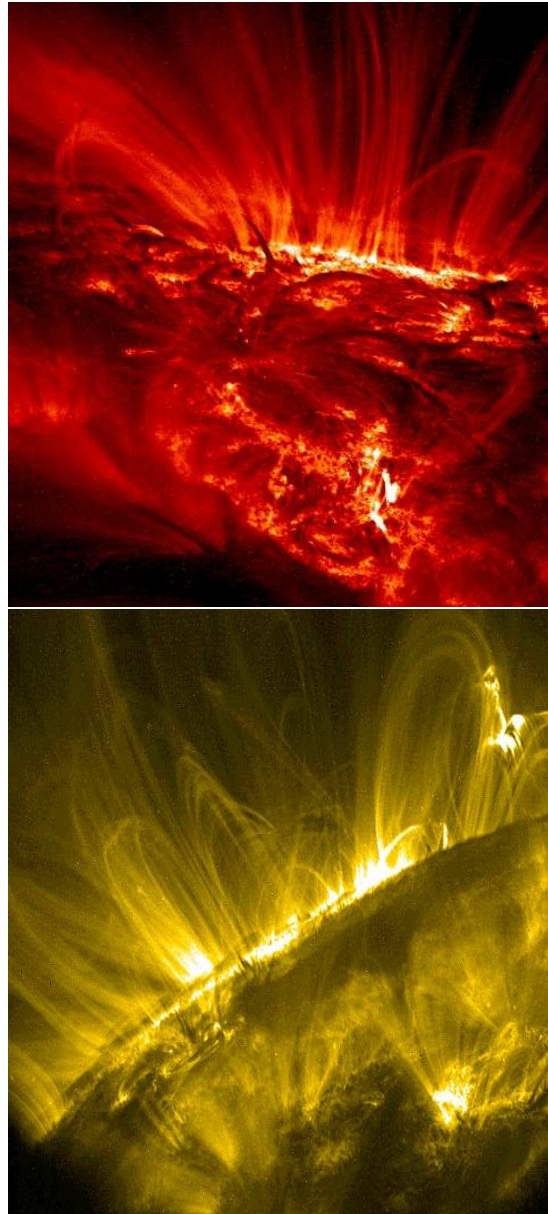


**Figure 1.** TRACE photos of numerous loops in active regions, with clear density structures.

tween ion and electron temperatures (typically  $T_i > T_e$ ), 5) explain the origin of the large temperature anisotropy ( $T_{\perp} > T_{\parallel}$ ) with respect to the direction of the magnetic field, particularly for ions, 6) explain the observed larger heating of heavier ions, and last but not least, 7) it should work everywhere in corona (with well known different heating requirements in active and quiet regions).

In this paper, we present a new coronal heating model that can operate in all layers and in all magnetic structures of the solar atmosphere and that is able to explain all seven requirements given above. Our model represents a *new paradigm* in which a) the energy for driving the drift modes and for the heating of corona is already present in corona, and, b) this energy is naturally transmitted to the different plasma species by well known effects that are, however, be-

yond the standardly used models and theories. Moreover, it is based on well established, basic theory which has already been verified and confirmed by means of laboratory plasma experiments. All that is needed for the heating mechanism to work is the presence of a density gradient perpendicular to the magnetic field. In the solar corona, this may be taken rather as a fact than as a hypothesis.

## 2 INHOMOGENEOUS SOLAR PLASMA

Fine density filaments and threads in the solar atmosphere have been observed for a long time now, even from ground-based observations like those during the eclipse in 1991 (November & Koutchmy 1997), showing a slow radial enlargement of plasma structures. On the other hand, measurements by Voyager 1 and Voyager 2 show (Woo & Habbal 1997) that the finest structures in the slow solar wind at around  $9 R_{\odot}$  are about 3 times finer than those in the fast wind. Assuming a radial expansion, these authors conclude that the transverse sizes of these highly elongated structures at the Sun are below 1 km. The contour maps presented in Karowska & Habbal (1991) reveal the existence of numerous structures of various size. The smallest filamentary structures of the order of 1 km have been discussed also in Woo (1996). Recent Hinode observations (De Pointieu et al. 2007) confirm that the solar atmosphere is a highly structured and inhomogeneous system and revealed radially spreading grass-like density filaments of various size pervading the whole domain. A very recent three-dimensional analysis (Aschwanden et al. 2008a) of coronal loops reveals short-scale density irregularities within each loop separately. Particularly clear images of coronal loops with density structures may be seen in Aschwanden et al. (2008b) and also in Warren et al. (2008). In Fig. 1 we give some TRACE images showing many coronal loops in active regions. Such active regions do not cover the whole corona, yet the analysis from Aschwanden (2001) reveals that they require around 82% of the total energy needed to heat the entire corona.

The presence of plasma density irregularities throughout the corona implies a plasma that is not in thermodynamic equilibrium. In other words, it reveals the presence of free energy in the system. In all the examples mentioned above, such density irregularities are as rule associated with the magnetic field, creating the ideal environment for drift waves. The purpose of this work is to show that the energy stored in these density gradients may drive drift waves on massive scales. We shall point out some basic features of the drift wave instability, apply them throughout the solar atmospheric plasma and compute the appropriate growth rates. It will be shown that the growing drift wave and its subsequent interaction with plasma particles may yield the long searched solution of the problem of the heating of the solar atmosphere. The model implies that the direct energy supply for the heating comes from within the corona itself, though still maintained and replenished by some mechanisms from below the photosphere. Those include a continuous restructuring of the magnetic field implying the consequent similar changes of the plasma density (due to the frozen-in condition), and also the observed inflow of the plasma along the magnetic loops (Schrijver et al. 1999). To some extent, this

looks similar to the currently accepted scenarios mentioned above, where the magnetic field plays an essential role and is assumed as given. However, in this new approach the dissipation of these drift waves is easy to explain in our kinetic model that works on the (very small) length scales at which the actual dissipation takes place.

The observable characteristic dimensions of the density irregularities are limited by the available resolution of the instruments (about 0.5 arcsecond in the example from Fig. 1, that is below 400 km on the Sun). Nevertheless, even extremely short, meter-size scales can not be excluded, especially in corona (Vranjes & Poedts 2008a). This can be seen by calculating the perpendicular ion diffusion coefficient (Chen 1988) for a coronal environment:  $D_{\perp,j} \approx \kappa T_j \nu_j / (m_j \Omega_j^2) \propto m_j^{1/2}$ , where  $j = i, e$ . Taking  $B_0 = 10^{-2}$  T,  $n_0 = 10^{15} \text{ m}^{-3}$ , and  $T_e = T_i = 10^6$  K, for ions we obtain  $D_{\perp,i} = 0.01 \text{ m}^2/\text{s}$ . The diffusion velocity in the direction of the given density gradient is (Vranjes & Poedts 2006)  $D_{\perp,j} \nabla n_0 / n_0$  [see also Eq. (3) further in the text]. Taking the inhomogeneity scale-length  $L_n \equiv [(dn_0/dx)/n_0]^{-1} = 10, 10^2, \text{ and } 10^5 \text{ m}$ , where  $x$ -denotes the direction perpendicular to the magnetic field vector, we obtain for the ion diffusion velocities, respectively,  $10^{-3}, 10^{-4}, \text{ and } 10^{-7} \text{ m/s}$  only. Therefore, even very short density inhomogeneities can last long enough to support relatively high frequency drift instabilities. Hence, in dealing with the drift wave, we may operate with the density inhomogeneity scale lengths that have any value ranging from one meter up to thousands of kilometers in the case of coronal plumes.

## 3 DRIFT WAVE WITHIN FLUID THEORY

Assuming a partially/weakly ionized and collisional plasma, like in the photosphere and chromosphere, it is justified to employ the fluid model. In such an environment, the kinetic Landau damping is not expected to play any significant role as long as the ion mean free path is below the wavelength. The strong-weak Landau damping transition has been experimentally verified (D'Angelo 1968) to be at the threshold  $\omega \sim \nu_i$ . The momentum equations that we use for electrons and ions can be written as

$$m_i n_i \left[ \frac{\partial \vec{v}_i}{\partial t} + (\vec{v}_i \cdot \nabla) \vec{v}_i \right] = e n_i (-\nabla \phi + \vec{v}_i \times \vec{B}_0) - \kappa T_i \nabla n_i - \nabla \cdot \pi_i - m_i n_i \nu_i \vec{v}_i, \quad (1)$$

and

$$0 = -e n_i (-\nabla \phi + \vec{v}_e \times \vec{B}_0) - \kappa T_e \nabla n_e - m_e n_e \nu_e \vec{v}_e, \quad (2)$$

respectively. Here,  $\nu_i \equiv \nu_{in}$  and  $\nu_e = \nu_{en} + \nu_{ei}$ . The ion momentum change due to collisions with electrons is neglected in view of the mass difference. This is justified as long as the ion dynamics in the direction of the magnetic field vector is negligible. Otherwise it may modify the instability threshold (Vranjes & Poedts 2008b). The shape of the equations reveals that we are dealing with electrostatic perturbations, the hot ion effects are included through the pressure and the *gyro-viscosity* stress tensor terms, while the left-hand side of the electron momentum equation is omitted, implying perturbations with phase speed and perturbed velocity both much below the electron thermal velocity. The dynamics of

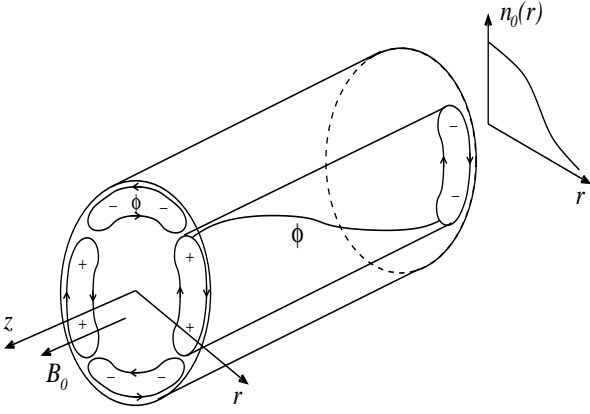


**Figure 2.** A drift wave in cylindrical geometry with poloidal wave number  $m = 2$ .

the neutrals may also be included. However, as shown elsewhere (Vranjes & Poedts 2009), this usually yields small or negligible corrections, and such a model works well as long as the ion sound response is negligible. Otherwise, there is an instability threshold that is modified when the dynamics of the neutrals is self-consistently included (Vranjes & Poedts 2008b). A typical geometry of the drift wave in cylindrical coordinates is presented in Fig. 2. Here, as an example we consider a wave propagating in the poloidal and axial directions, with the poloidal mode number  $m = 2$ , in a plasma with a radially dependent equilibrium density. The actual wave fronts are twisted around the axis and have an  $r$ -dependent amplitude which reaches a maximum in the area of the largest density gradient. The mode behavior in the presence of both radial and axial equilibrium density gradients is discussed in Vranjes & Poedts (2007).

In some regions, the drift mode may become electromagnetic, provided the plasma  $\beta$  exceeds the electrostatic limit. This yields a coupling of the drift and the kinetic Alfvén wave (Kadomtsev 1965; Vranjes & Poedts 2006). The first *experimental observation* of such a coupled mode in a hot-ion plasma is discussed in Nishida & Ishii (1974). The drift-wave part of the observed coupled modes, is strongly growing, and the maximum growth rate  $\omega_i \simeq 0.1 \omega_r$ , where  $\omega_r$  is the drift wave frequency. In the case of the lower solar atmosphere, as shown in Vranjes & Poedts (2006), the Alfvén part of the mode is of no interest as it is always damped due to the collisions, and it will not be discussed here. Note that the usual gas viscosity is as a rule negligible even for a relatively high density environment like the photosphere and chromosphere. More details are available in Vranjes et al. (2008a).

The ion gyro-viscous components of the stress tensor that we need here are (Weiland 2000)

$$\pi_{xy} = \pi_{yx} = \frac{n_i \kappa T_i}{2\Omega_i} \left( \frac{\partial v_{ix}}{\partial x} - \frac{\partial v_{iy}}{\partial y} \right),$$

$$\pi_{yy} = -\pi_{xx} = \frac{n_i \kappa T_i}{2\Omega_i} \left( \frac{\partial v_{iy}}{\partial x} + \frac{\partial v_{ix}}{\partial y} \right).$$

Here and further we have taken  $\vec{B}_0 = B_0 \vec{e}_z$ , and  $v_{Ti}^2 = \kappa T_i / m_i$ .

The ion perpendicular velocity obtained from Eq. (1) is described by the following recurrent formula

$$v_{i\perp} = \alpha_i \left[ \frac{1}{B_0} \vec{e}_z \times \nabla_{\perp} \phi + \frac{v_{Ti}^2}{\Omega_i} \vec{e}_z \times \frac{\nabla_{\perp} n_i}{n_i} - \frac{\nu_i}{\Omega_i} \frac{\nabla_{\perp} \phi}{B_0} - \frac{\nu_i v_{Ti}^2}{\Omega_i^2} \frac{\nabla_{\perp} n_i}{n_i} + \vec{e}_z \times \frac{\nabla_{\perp} \cdot \pi_i}{m_i n_i \Omega_i} + \frac{1}{\Omega_i} \left( \frac{\partial}{\partial t} + \vec{v}_i \cdot \nabla \right) \vec{e}_z \times \vec{v}_{i\perp} - \frac{\nu_i}{\Omega_i} \frac{\nabla_{\perp} \cdot \pi_i}{en_i B_0} - \frac{1}{\Omega_i} \frac{\nu_i}{\Omega_i} \left( \frac{\partial}{\partial t} + \vec{v}_i \cdot \nabla \right) \vec{v}_{i\perp} \right]. \quad (3)$$

Here,  $\alpha_i = 1/(1 + \nu_i^2/\Omega_i^2)$ . The velocity can be calculated up to small terms of any order using the drift approximation  $|\partial/\partial t| \ll \Omega_i$ .

### 3.1 Ion diamagnetic current effects

The ion gyro-viscosity is usually overlooked in the literature and, in particular, in the domain of solar plasma, and this even in studies using the multi-component plasma theory. For the solar plasma case, this may have very important consequences because ion and electron temperatures are typically of the same order, so that a cold ion approximation and the consequent neglect of the ion gyro-viscosity can not be justified.

As a matter of fact, it is well known (Vranjes & Poedts 2006; Weiland 2000) (yet standardly disregarded) that part of the ion gyro-viscosity contributes to the cancelation of some terms in the ion continuity equation. Clearly, this implies that, if the gyro-viscosity terms are omitted in the derivation, the resulting ion equations contain terms that can not possibly be there, yielding some false physical effects. The cancelation of terms appears when Eq. (3) is set into the ion continuity  $\partial n_i / \partial t + \nabla_{\perp} \cdot (n_i v_{i\perp}) + \nabla_z \cdot (n_i v_{iz}) = 0$ , and it involves, respectively, the diamagnetic and polarization drifts from one side

$$\vec{v}_{*i} = \frac{v_{Ti}^2}{\Omega_i} \vec{e}_z \times \frac{\nabla_{\perp} n_i}{n_i}, \quad \vec{v}_{pi} = \frac{1}{\Omega_i} \left( \frac{\partial}{\partial t} + \vec{v}_i \cdot \nabla \right) \vec{e}_z \times \vec{v}_{i\perp},$$

and the stress tensor drift term  $\vec{v}_{\pi i} = \vec{e}_z \times \nabla_{\perp} \cdot \pi_i / (m_i n_i \Omega_i)$  from the other side.

It is seen that, as long as the magnetic field is homogeneous, we have

$$\nabla \cdot (n_i \vec{v}_{*i}) \equiv 0, \quad (4)$$

describing a well known fundamental property. This is due to the fact that the diamagnetic drift is a fluid effect and not a particle drift, and therefore it can not contribute to the flux in the continuity equation. It appears due to the gyration of ion particles in the presence of density gradient, and without any macroscopic motion of the ion guiding center. However, if an inappropriate linearization is done, it gives rise to the terms  $(\vec{k} \cdot \vec{v}_{*i}) n_{i\perp}$  in the continuity equation, that provides a false source of the current-driven instability that may be seen in the literature.

The mentioned cancelation of terms is due to the convective derivative part

$$(\vec{v}_i \cdot \nabla) \vec{e}_z \times \vec{v}_{i\perp} \quad (5)$$

in the polarization drift  $\vec{v}_{pi}$ . The procedure is described in detail in Vranjes & Poedts (2006); Weiland (2000). Within

the approximation of small gradients of the equilibrium quantities, the last  $\vec{v}_{i\perp}$  in the convective derivative (5) contains only the leading order perturbed drifts from Eq. (3). On the other hand, the first  $\vec{v}_i$  in (5) can only be the equilibrium ion diamagnetic drift. This is then to be used in the term  $\nabla_{\perp} \cdot (n_i \vec{v}_{pi})$  in the continuity equation.

The stress tensor drift term yields

$$\nabla_{\perp} \cdot (n \vec{v}_{\pi}) = -\rho_i^2 \nabla_{\perp} n_{i0} \cdot \nabla_{\perp}^2 \vec{v}_{i\perp} - n_{i0} \rho_i^2 \nabla_{\perp}^2 \nabla_{\perp} \cdot \vec{v}_{i\perp}. \quad (6)$$

Here,  $\rho_i = v_{Ti}/\Omega_i$ . Within the second-order small terms approximation, the first term on the right-hand side in this expression *cancels out exactly* with the contribution of the above discussed convective derivative in the polarization drift  $\nabla_{\perp} \cdot [n(\vec{v}_i \cdot \nabla) \vec{e}_z \times \vec{v}_{i\perp}]$ . The cancelation of terms is exact and valid for any plasma. Moreover, the results obtained from this formal fluid theory can easily be obtained by using the kinetic theory as well [cf. Vranjes & Poedts (2006); Weiland (2000)]. However, if the derivation is performed incorrectly, by simply ignoring the stress tensor contribution, then the resulting equations contain extra terms originating from the convective derivative in the ion polarization drift. For perturbations of the form  $\sim \exp(-i\omega t + ik_y y + ik_z z)$  this implies the presence of terms like  $\vec{k} \cdot \vec{v}_{*i}$ , which in reality cancel out exactly. A drastic example where a false 'new instability' is obtained due to these terms may be seen in Mecheri & Marsch (2008).

### 3.2 Dissipative instability

In the limit of perturbations with a parallel (to the magnetic field vector) phase velocity that is considerably larger than the sound speed  $\omega/k_z \gg c_s = (\kappa T_e/m_i)^{1/2}$ , the ion continuity equation reads (Vranjes & Poedts 2006):

$$\begin{aligned} & \frac{\partial}{\partial t} \left( \frac{n_{i1}}{n_{i0}} \right) + \frac{1}{B_0} \vec{e}_z \times \nabla_{\perp} \phi_1 \cdot \frac{\nabla_{\perp} n_{i0}}{n_{i0}} \\ & - \nu_i \rho_i^2 \nabla_{\perp}^2 \left( \frac{e\phi_1}{\kappa T_i} + \frac{n_{i1}}{n_{i0}} \right) - \rho_i^2 \frac{\partial}{\partial t} \nabla_{\perp}^2 \left( \frac{e\phi_1}{\kappa T_i} + \frac{n_{i1}}{n_{i0}} \right) \\ & + \frac{\rho_i^2}{\Omega_i} \frac{\partial}{\partial t} \nabla_{\perp}^4 \left( \frac{\phi_1}{B_0} + \frac{v_{Ti}^2 n_{i1}}{\Omega_i n_{i0}} \right) = 0. \end{aligned} \quad (7)$$

Here, the discussion from the previous section is included self-consistently. For the assumed shape of perturbations, Eq. (7) yields:

$$\frac{n_{i1}}{n_{i0}} = -\frac{\omega_{*i} + \omega \rho_i^2 k_y^2 (1 + \rho_i^2 k_y^2) + i\nu_i \rho_i^2 k_y^2 e\phi_1}{\omega [1 + \rho_i^2 k_y^2 (1 + \rho_i^2 k_y^2)] + i\nu_i \rho_i^2 k_y^2 \kappa T_i}, \quad (8)$$

$$\omega_{*i} = k_y \frac{v_{Ti}^2 n'_{i0}}{\Omega_i n_{i0}}, \quad \nabla_{\perp} n_{i0} = -\vec{e}_x n'_{i0} = -\vec{e}_x dn_{i0}/dx.$$

The electron perpendicular and parallel velocities are obtained from Eq. (2):

$$\begin{aligned} v_{e\perp} &= \frac{1}{1 + \nu_{en}^2/\Omega_e^2} \left[ \frac{1}{B_0} \vec{e}_z \times \nabla_{\perp} \phi + \frac{\nu_{en}}{\Omega_e} \frac{\nabla_{\perp} \phi}{B_0} \right. \\ & \left. - \frac{v_{Te}^2 \nu_{en}}{\Omega_e^2} \frac{\nabla_{\perp} n_e}{n_e} - \frac{v_{Te}^2}{\Omega_e} \vec{e}_z \times \frac{\nabla_{\perp} n_e}{n_e} \right]. \end{aligned} \quad (9)$$

$$v_{ez1} = \frac{ik_z v_{Te}^2}{\nu_{en}} \left( \frac{e\phi_1}{\kappa T_e} - \frac{n_{e1}}{n_{e0}} \right). \quad (10)$$

From the electron continuity we then obtain

$$\frac{n_{e1}}{n_{e0}} = \frac{\omega_{*e} + iD_p + iD_z}{\omega + iD_p + iD_z} \frac{e\phi_1}{\kappa T_e}. \quad (11)$$

Here  $D_p = \nu_e k_y^2 \rho_e^2$ ,  $D_z = k_z^2 v_{Te}^2 / \nu_e$ ,  $\rho_e = v_{Te}/\Omega_e$ , and

$$\omega_{*e} = -k_y \frac{v_{Te}^2 n'_{e0}}{\Omega_e n_{e0}}.$$

The term  $D_p$  describes the usually neglected effects of electron collisions in the perpendicular direction. In most cases, in view of the small inertia, these electron collision effects are included from the electron parallel momentum. This is justified provided that (Vranjes & Poedts 2006)

$$k_z^2 \Omega_e^2 / (k_y^2 \nu_e^2) \gg 1. \quad (12)$$

In solar plasmas, for perturbations with an almost arbitrarily small parallel wave number this condition may not always be satisfied. This means that collisions must be taken into account in the perpendicular dynamics.

In the absence of an equilibrium electric field and for quasi-neutral perturbations, the dispersion equation of the drift mode in collisional solar plasma is:

$$\begin{aligned} & \frac{T_e}{T_i} \frac{\omega_{*i} + \omega \rho_i^2 k_y^2 (1 + \rho_i^2 k_y^2) + i\nu_i \rho_i^2 k_y^2}{\omega [1 + \rho_i^2 k_y^2 (1 + \rho_i^2 k_y^2)] + i\nu_i \rho_i^2 k_y^2} \\ & + \frac{\omega_{*e} + i(D_p + D_z)}{\omega + i(D_p + D_z)} = 0. \end{aligned} \quad (13)$$

In various limits, Eq. (13) yields different dispersion equations for the drift wave known from the literature.

The most simple case is for collision-less plasma, when the right-hand side in Eq. (13) reduces to 1. Assuming, in addition, that  $1 \gg \rho_i^2 k_y^2$ , we have

$$\omega_r = \omega_{*e} / (1 + \rho_s^2 k_y^2), \quad \rho_s = c_s / \Omega_i, \quad c_s^2 = \kappa T_e / m_i. \quad (14)$$

In the case of cold ions and for  $D_z \gg D_p$ , we obtain from Eq. (13) the same oscillation frequency as in the previous example. But the growth rate due to electron collisions is (Vranjes & Poedts 2008b; Weiland 2000)

$$\gamma = \frac{\nu_e \omega_r^2 \rho_s^2 k_y^2}{k_z^2 v_{Te}^2}. \quad (15)$$

As mentioned earlier, this describes the drift mode growing in the presence of electron collisions. The full Eq. (13) can be solved numerically, taking relevant parameters for the solar atmosphere at various altitudes (Vranjes & Poedts 2006). The result represents an interplay between the ion collisions that damp the mode, and the electron collisions that produce the growth rate approximately given by Eq. (15). This may have a great importance in terms of plasma heating because the wave is always present in inhomogeneous plasmas, while in the same time the wave energy is continuously absorbed by the collisions of heavy species. The process continues till it runs out of energy. In other words, it continues as long as the source (i.e., the density gradient) is present.

## 4 KINETIC INSTABILITY OF DRIFT WAVE

In most of the corona the collisions are not expected to play an important role and consequently the drift dissipative instability may not be of much importance. In addition, regarding the problem of coronal heating as a background

and motivation for any wave analysis, in the case of so limited collisions an efficient mechanism for transfer of energy from the wave to plasma is missing. However, this is not so within the frame of the drift wave kinetic theory. In that case, the process develops as follows: the interaction of the wave and electrons is destabilizing and the mode grows due to Cherenkov-type interaction (in the presence of the density gradient), while in the same time its energy is absorbed by ions due to Landau damping. This may be seen from Weiland (2000); Ichimaru (1980) where, under the conditions

$$k_z v_{Ti} \ll \omega \ll k_z v_{Te}, \quad \omega \ll \Omega_i, \quad \frac{|k_y|}{|k_z|} \frac{\rho_i}{L_n} \left( \frac{T_e}{T_i} \right)^{1/2} \gg 1, \quad (16)$$

the wave properties are described by the frequency

$$\omega_r = - \frac{\omega_{*i} \Lambda_0(b_i)}{1 - \Lambda_0(b_i) + T_i/T_e + k_y^2 \lambda_{di}^2}, \quad (17)$$

and the corresponding growth rate

$$\begin{aligned} \gamma \simeq & - \left( \frac{\pi}{2} \right)^{1/2} \frac{\omega_r^2}{|\omega_{*i}| \Lambda_0(b_i)} \left[ \frac{T_i}{T_e} \frac{\omega_r - \omega_{*e}}{|k_z| v_{Te}} \exp[-\omega_r^2 / (k_z^2 v_{Te}^2)] \right. \\ & \left. + \frac{\omega_r - \omega_{*i}}{|k_z| v_{Ti}} \exp[-\omega_r^2 / (k_z^2 v_{Ti}^2)] \right]. \quad (18) \end{aligned}$$

Here,

$$\Lambda_0(b_i) = I_0(b_i) \exp(-b_i), \quad b_i = k_y^2 \rho_i^2, \quad \lambda_{di} = v_{Ti} / \omega_{pi},$$

and  $I_0$  is the modified Bessel function of the first kind and of the order 0. The first condition in (16) refers to the use of approximative expressions for the plasma dispersion function, while the second condition implies a strongly magnetized plasma, and the third implies that the acoustic part in the dispersion equation can be omitted. Eqs. (17) and (18), as well as Eq. (13), are obtained using a local approximation. This implies that the characteristic length for the change of the mode amplitude in the direction of the density gradient, is much larger than the perpendicular wavelength, i.e.,  $(d/dx)^{-1} \simeq L_n \gg \lambda_y$ . Otherwise, an eigen-mode analysis is to be used, see for more details in Vranjes & Poedts (2004) and Vranjes & Poedts (2007). Note that in the appropriate limits ( $k_y^2 \lambda_{di}^2 \ll 1$ ,  $b_i \ll 1$ ) Eqs. (14) and (17) coincide. In Eq. (18), the last term in the square bracket is positive. It describes the damping on ions and introduces a threshold in the mode instability that is of importance only in plasmas with hot ions, yet negligible as long as  $\omega_r/k_z \gg v_{Ti}$  (hence the reason for interest in small  $k_z$ ). The necessary condition for the instability follows from the first term where we must have  $\omega_r < \omega_{*e}$ , that is as a rule easily satisfied. Equations (14) and (17) reveal the presence of the energy source already in the real part of the frequency  $\omega_r \propto \nabla_{\perp} n_0$ , while details of its growth due to the same source are described by Eqs. (15) and (18).

As an example, in Fig. 3 the growth rate (18) is calculated for an electron-proton plasma in terms of the parallel wavelength  $\lambda_z$  by taking  $B_0 = 10^{-2}$  T,  $n_0 = 10^{15}$  m $^{-3}$ ,  $L_n = [(dn_0/dx)/n_0]^{-1} = s \cdot 100$  m, and for  $\lambda_y = 0.1, 0.3, 0.5$ , and 1 m. Because  $k_y \gg k_z$ , the corresponding wave frequencies are practically constant and have approximate values 186, 210, 254, and 307 Hz, respectively (this assuming  $s = 1$ , but see below). In all these cases, we have very strongly growing drift modes. Note that in all four cases

**Figure 3.** The growth rate (18) normalized to the wave frequency  $\omega_r$  in terms of the parallel wavelength, for several perpendicular wavelengths  $\lambda_y$ , and for the density scale-length  $L_n = s \cdot 100$  m,  $s \in (0.1, 10^3)$ .

$\omega_r < \omega_{*e}$ , and the growth rate changes sign because of the varying (with  $\lambda_z$ ) contribution of the ion part in Eq. (18). Observe the extremely fast growth for short perpendicular wavelengths  $\lambda_y$ . The growth rate increases with  $\lambda_z$  and may easily become much larger than  $\omega_r$ . Yet, strictly speaking, in that case the assumption of smallness of the imaginary part with respect to the real part, used in the expansion of the plasma dispersion function, is violated, and the problem must be treated numerically. In the examples presented in Fig. 3, the conditions used in obtaining Eq. (18) are formally well satisfied, i.e.,  $\omega_r \ll \Omega_i$  and in the given range of  $k_z$ , we have  $k_z v_{Ti} < \omega_r < k_z v_{Te}$ , and also the sound branch is always far below the drift branch. For the given parameters, the Debye length  $\lambda_d$  is around 1 mm only, and even shorter values of  $\lambda_y$  are permissible. The local approximation is also well satisfied and the mode growth is expected to take place throughout the density gradient. For the given density, the plasma- $\beta$  is around  $0.6 m_e/m_i$ .

A simple way to demonstrate that a similar mode behavior can take place at various inhomogeneity scale-lengths  $L_n$  (in other words at various places in the corona), is to keep the ratio  $\lambda_z/L_n$  fixed. Thus, with the same parameters as above we set  $L_{n1} = s \cdot L_n$ ,  $\lambda_{z1} = s \cdot \lambda_z$ , where  $s$  takes values, e.g., between 0.1 and  $10^3$ . It can easily be shown that the graphs from Fig. 3 remain *exactly the same*. In other words, the ratio  $\gamma/\omega_r$  remains unchanged, although both  $\gamma$  and  $\omega_r$  are shifted towards lower values. For example, for  $s = 10^3$ , i.e.,  $L_{n1} = 10^5$  m,  $\lambda_{z1} = 10^7$  m, and taking  $\lambda_y = 0.5$  m, we have  $\gamma/\omega_r = 0.26$ . This is the same as the value of the line labeled *c* in Fig. 3, for  $\lambda_z = 10$  km (and correspondingly  $L_n = 100$  m). Yet, now  $\gamma = 0.07$  Hz, and  $\omega_r = 0.25$  Hz. Such a variation of  $s$  may be used to describe the natural change of the radial density gradient when we move *along* a magnetic flux tube, that may appear due to the diverging tube geometry. So the mode growth occurs everywhere along the given flux tube. Hence, as long as the conditions (16) used in the derivations are satisfied, the results in Fig. 3 are valid for any  $s$  in the range  $0.1 - 10^3$ .

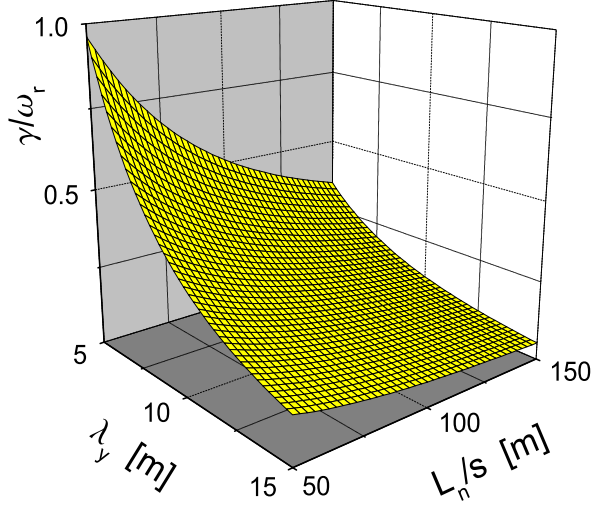


**Figure 4.** The growth rate (18) normalized to  $\omega_r$  in terms of the perpendicular wavelength, for several values of  $\lambda_z$ .

**Figure 6.** The growth rate (18) normalized to the wave frequency  $\omega_r$  in terms of the perpendicular wavelength  $\lambda_y$  and the density scale-length  $L_n$ , for  $\lambda_z = s \cdot 2 \cdot 10^4$  m,  $s \in (0.1, 10^3)$ .

**Figure 5.** The growth rate (18) normalized to  $\omega_r$  in terms of the density scale length  $L_n$  for several values of  $\lambda_z$ ,  $s \in (0.1, 10^3)$ .

Next, we check the mode behavior with respect to the perpendicular wavelength  $\lambda_y$ . We fix  $L_n = s \cdot 100$  m, keep the other parameters the same as above, and calculate the growth rate for  $\lambda_z/s = 7, 10$ , and  $15$  km. The result is presented in Fig. 4. The graphs and the damping in the short  $\lambda_y$  range (for  $\lambda_z = 7$  m) are in agreement with Fig. 3.

In Fig. 5 we present the mode growth rate in terms of  $L_n$ , for the same plasma parameters as above. The graphs remain unchanged for any  $s \in (0.1, 10^3)$ . The frequency is 507 Hz (at  $L_n = 50$  m), and 254 Hz (at  $L_n = 170$  m), for  $s = 1$ . In the case  $s = 10^3$ , the frequency is 0.5 Hz (where now  $L_n = 50$  km), and 0.15 Hz (at  $L_n = 170$  km).

A similar quantitative analysis may be performed for densities several orders of magnitude below the used value, and for at least one order of magnitude higher density as well, resulting in the same wave behavior, with only some shift in the wave frequencies and wavelengths. This is seen

from Fig. 6, where the growth rate is plotted in terms of  $\lambda_y$  and  $s \cdot L_n$  by taking  $n_0 = 10^{13} \text{ m}^{-3}$ ,  $B_0 = 10^{-3} \text{ T}$ , and  $\lambda_z = s \cdot 2 \cdot 10^4$  m. The smaller values of  $n_0$  and  $B_0$  imply the possible application of the model to higher altitudes in the corona. It is seen that the perpendicular wavelength is just shifted up for one order of magnitude, and the growth rate decreases with  $\lambda_y$  and  $L_n$  just like in Figs. 4 and 5.

On the other hand, for densities that are two or more orders of magnitude larger than the earlier used value  $10^{15} \text{ m}^{-3}$ , and thus for a larger plasma- $\beta$ , a coupling with electromagnetic Alfvén-type perturbations may take place (Hasegawa 1975). As shown elsewhere (Vranjes & Poedts 2006), the drift mode behavior will remain similar even in that case. The frequency becomes slightly reduced and a part of the wave energy is spent on the coupling with this additional Alfvén mode that appears to be always damped by collisions. This coupling is described by the following dispersion equation (Weiland 2000; Vranjes & Poedts 2006)

$$\omega^3 - \omega^2(\omega_{*e} + \omega_{*i}) + \omega[\omega_{*e}\omega_{*i} - k_z^2 c_a^2 / (1 + k_y^2 \rho_i^2) - k_y^2 k_z^2 c_a^2 (\rho_i^2 + \rho_s^2)] + k_z^2 c_a^2 \omega_{*e} / (1 + k_y^2 \rho_i^2) = 0. \quad (19)$$

Here,  $c_a^2 = B_0^2 / (\mu_0 n_0 m_i)$ . The nature of coupling is best seen for negligible ion thermal effects when we have  $(\omega - \omega_{*e})(\omega^2 - k_z^2 c_a^2) - \omega k_z^2 c_a^2 k_y^2 \rho_s^2 = 0$ . For sufficiently small  $k_y^2 \rho_s^2$ , the two modes propagate practically almost independently.

In view of all these results, we stress again an important difference of the drift wave as compared to other plasma modes. The mode frequency given by Eq. (17), already by its form *implies* the presence of an energy source stored in the density gradient. This free energy is then responsible for its growth, either due to kinetic or fluid effects, and the details of the growth are described by Eqs. (15) and (18). Compare this with, e.g., an Alfvén  $\omega = kc_a$ , or a sound mode  $\omega = kc_s$ , where the given dispersion equations only allow for the *possibility* for the plasma to support these modes, on the condition that an *additional* energy source is provided.

As for the experimental verification of such a very strongly growing drift-wave instability, one (out of many)

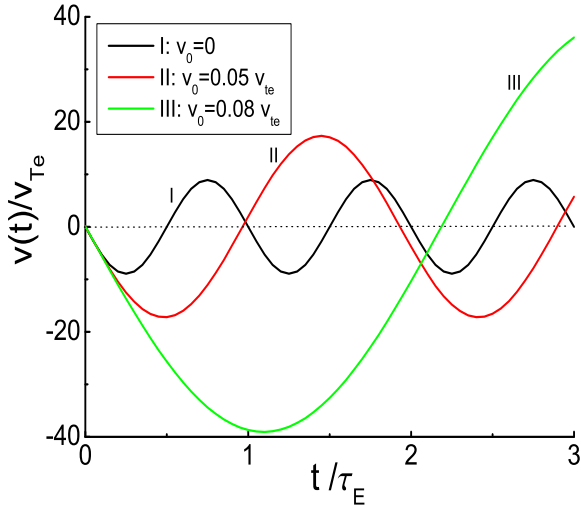


**Figure 7.** Velocity of electrons (20) accelerated by the drift-wave electric field with  $\phi = 80$  V, for three different starting velocities.

may be found e.g., in Brossier et al. (1971) for a similar almost collision-less *hydrogen* plasma with  $T_e = 14$  eV,  $T_i = 2$  eV,  $B_0 \leq 0.35$  T, and the density  $n_0 = 10^{16}$  m $^{-3}$ . Note that in the experiment the maximum observed linear growth-rate was very high:  $\omega_i \simeq \omega_r = 7 \cdot 10^5$  Hz.

#### 4.1 Electron acceleration by parallel wave-electric field

The electrostatic drift mode presented in Figs. 3-6 implies a time-varying electric field, whose parallel component  $|\nabla_z \phi|/E_d = |k_z \phi|/E_d$ , normalized to the Dreicer runaway electric field, for  $\lambda_z = 10$  km and  $\phi = 60, 80$  V/m, is 3.1 and 4.1, respectively. Here, we use  $\lambda_y = 0.5$  m,  $B_0 = 10^{-2}$  T,  $n_0 = 10^{15}$  m $^{-3}$ ,  $L_n = [(dn_0/dx)/n_0]^{-1} = 100$  m, and the reason for the given values of  $\phi$  will be given in the forthcoming sections. The Dreicer electric field is (Dreicer 1959)  $E_d = eL_{ei}/(4\pi\epsilon_0\lambda_d^2)$ . Here,  $L_{ei} = \log(\lambda_d/b_0)$  is the Coulomb logarithm,  $\lambda_d = \lambda_{de}\lambda_{di}/(\lambda_{de}^2 + \lambda_{di}^2)^{1/2}$  is the plasma Debye radius, and  $b_0 = [e^2/[12\pi\epsilon_0\kappa(T_e + T_i)]]^{-1}$  is the impact parameter for electron-ion collisions Vranjes et al. (2008b). For the given temperature of one million K, we have  $L_{ei} = 20.1$ ,  $\lambda_d = 0.0015$  m, and the Dreicer field is 0.012 V/m. Hence, the parallel wave field exceeds the Dreicer field so that the bulk plasma species (primarily electrons) can be accelerated/decelerated by the wave in the parallel direction. The acceleration is more effective on particles that are already more energetic, resulting in a distribution function considerably different from a Maxwellian. This may be one of the reasons behind the observed kappa-distribution in the outer solar atmosphere and in the solar wind.

For  $s = 10^3$  and for the two values of  $\phi$  mentioned above, the normalized electric field is 0.003 and 0.004, respectively. For such small normalized values, and also in view of the fact that the electron mean-free-path is orders of magnitude below the parallel wave-length, the effect of the acceleration on the bulk electrons is negligible.

The electron parallel velocity in such a time-varying

wave-electric field  $E_0 \cos(k_z z - \omega_r t)$ , is approximately given by Bittencourt (1995)

$$v(t) = v_0 - \frac{eE_z}{m_e(k_z v_0 - \omega_r)} \{ \sin[k_z z_0 + (k_z v_0 - \omega_r)t] - \sin(k_z z_0) \}. \quad (20)$$

Here,  $v_0$  and  $z_0$  are the starting electron velocity and position in the parallel direction, respectively. Clearly, the acceleration of every separate particle is dependent on its particular velocity  $v_0$ , the lowest being for those with  $v_0 = 0$ . A strong acceleration will take place for resonant particles satisfying  $v_0 = \omega_r/k_z$  [see also in Fletcher & Hudson (2008)]. For the parameters used above  $\lambda_z = 10$  km and  $\lambda_y = 0.5$  m, we have  $\omega_r = 254$  Hz, and  $\gamma/\omega_r = 0.26$ . Thus, the resonant particles are those with  $v_0 = 404$  km/s  $\simeq 0.1v_{Te}$ .

The acceleration of electrons with different starting velocities is seen in Fig. 7, where the achieved velocity  $v(t)$  (normalized to  $v_{Te}$ ) is presented for three electron populations with  $v_0/v_{Te} = 0, 0.05$ , and  $0.08$ . The figure describes the different effective oscillation periods  $2\pi/(k_z v_0 - \omega_r)$  and the amplitudes of the three electron populations within the same wave period  $\tau_E = 2\pi/\omega_r = 0.025$  s of the electric field with  $\phi = 80$  V (which coincides with the electron population with  $v_0 = 0$ ).

The given time variation implies electron fluxes in both directions along the  $z$ -axis. For the line labeled III in Fig. 7, we have the electron velocity  $\Delta v \simeq 40v_{Te}$  corresponding to the energy of  $10^{-14}$  J, or around 69 keV. This oscillatory acceleration/deceleration is expected to considerably contribute to electron heating only if  $v_e \gg \omega_r$ . The process is also accompanied by a radiation, with the energy (Panofsky & Philips 1978) radiated by an electron

$$\frac{\Delta\Sigma}{\Delta t} = \frac{1}{4\pi\epsilon_0} \frac{2e^2}{3c^3} \frac{(\Delta v/\Delta t)^2 - (\vec{v} \times \Delta\vec{v}/\Delta t)^2/c^2}{(1 - v^2/c^2)^3}.$$

Setting as an example  $\Delta t = \tau_E$ , for this particular case we obtain a very small energy  $\Delta\Sigma = 1.4 \cdot 10^{-35}$  J radiated by an electron in one act of deceleration.

Because the wave-field is, in fact, created by the plasma particles, this acceleration/deceleration should have a feedback effect onto the wave itself. Clearly, it may affect the wave amplitude, especially for shorter wavelengths. In this case, the escaping electrons imply a lower amount of them remaining to shield the ion perturbations, and the perturbations should be increased. Yet, this all could be captured consistently only by numerical tools.

#### 4.2 Plasma heating by the drift wave

From Eq. (18), it is seen that for a wave frequency below  $\omega_{*e}$ , the dissipation rate can formally be written as  $\omega_i = |\gamma_{el}| - |\gamma_{ion}|$ , and two parallel mechanisms of plasma heating are in action here.

The term  $|\gamma_{ion}|$  is responsible for the Landau dissipation of the wave energy and, consequently, for the heating of the plasma. So, as long as the density gradient is present, there is a continuous precipitation of energy from the wave to the plasma. Note that similar heating due to the Landau dissipation of the ion acoustic mode (D'Angelo 1968) predicts a stronger heating of ions (Revathy 1977), in agreement with observations.

On the other hand, the term  $|\gamma_{el}|$  produces a growth of the wave, and this implies another (stochastic) heating mechanism that also involves single particle interaction with the wave. This is a process described and *experimentally verified* in McChesney et al. (1987); Sanders et al. (1998). For drift wave perturbations of the form  $\phi(x) \cos(k_y y + k_z z - \omega t)$ ,  $|k_y| \gg |k_z|$ , one finds the ion particle trajectory in the wave field from the following set of equations:

$$\begin{aligned} d\chi/d\tau &= \Upsilon, & \chi &= k_y x, & \Upsilon &= k_y y, & \tau &= \Omega_i t \\ d^2\Upsilon/d\tau^2 &= -\Upsilon + [m_i k^2 \phi / (e B_0^2)] \sin(\Upsilon - \tau \omega / \Omega_i). \end{aligned} \quad (21)$$

The analysis from Sanders et al. (1998) reveals that stochastic heating takes place for a sufficiently large wave amplitude, more precisely for

$$a = k_y^2 \rho_i^2 \frac{e\phi}{\kappa T_i} \geq 1. \quad (22)$$

The maximum achieved bulk ion velocity is shown to be proportional to the wave amplitude and is given by

$$v_{max} \simeq [k_y^2 \rho_i^2 e\phi / (\kappa T_i) + 1.9] \Omega_i / k_y. \quad (23)$$

Ideally, this requires

$$|\gamma_{el}| \geq |\gamma_{ion}|, \quad (24)$$

so that the wave amplitude may grow and at some point both heating mechanisms may take place, simultaneously. The condition (24) can easily be satisfied in view of the almost unlimited range of the parallel wave number  $k_z$ , so that the ion Landau damping can be made small, i.e.,  $|\omega/k_z| \gg v_{Ti}$ .

In the stochastic heating due to the drift wave, the ions move in the perpendicular direction to large distances and feel the time-varying field of the wave due to the polarization drift  $\vec{v}_p = (\partial \vec{E} / \partial t) / (\Omega_i B_0)$  [the sixth term in Eq. (3)], and as a result their motion becomes stochastic. In other words, the polarization drift of the ions becomes comparable to the  $\vec{E} \times \vec{B}$  drift, and the displacement due to the polarization drift is comparable to the wavelength. The single-ion motion becomes chaotic because of trapping (in the wave potential well) and de-trapping due to the magnetic field. The polarization drift is in the direction of the wave number vector, which emphasizes the crucial *electrostatic nature* of the wave in the given process of heating. Also important to stress is that in this scenario the stochastic heating is highly anisotropic, and it takes place mainly in the direction normal to the magnetic field  $B_0$  (both the  $x$ - and  $y$ -direction velocities are stochastic). In the same time, in view of the mass difference and the physical picture given above, this heating scenario predominantly acts on ions. The heating is maximal in the areas of strong density gradients (the areas of maximal drift wave activity), and also proportional to the strength of the magnetic field (the stronger the field the more localized heating). All these facts have been confirmed experimentally and, in the solar case, satisfy the observational constraints for the coronal heating mechanism discussed in the introduction.

As a matter of fact, in application to coronal plasma, the indication or proof that the described heating really takes place would be: i) an ion temperature anisotropy  $T_{i\perp} \gg T_{iz}$ , ii) a possibly higher ion temperature in comparison to electrons, and iii) a better heating of heavier ions. Observations show that i) may be taken rather as a rule than as

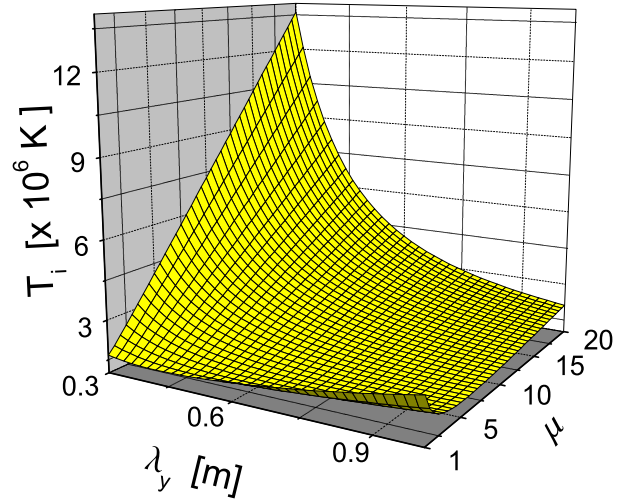


**Figure 8.** The stochastically increased ion temperature  $T_{eff} = m_i v_{max}^2 / (3\kappa)$  (in millions K) in terms of the perpendicular wavelength  $\lambda_y$  and the ion mass.

an exception [see in Li et al. (1998), Cuseri et al. (1999), Cranmer et al. (2008)], i.e., the perpendicular stochastic heating is more dominant compared to the parallel heating. This may also be expected from Fig. 3, where the Landau resonance  $\omega/k_z \sim v_{Ti}$  takes place for short wavelengths. For example, in the case of line  $c$  there, having  $v_{Ti} \simeq 91$  km/s, the ion resonance takes place at  $\lambda_z \simeq 2.2$  km, i.e., in the domain where the wave is strongly damped and will not appear at all. There are also numerous indications that confirm the features ii) and iii). As an example, we refer to graphs from Hansteen et al. (1997), where  $T_e < T_H < T_{He}$  throughout the corona and the solar wind. Similar results may also be seen in Cuseri et al. (1999) and Cranmer et al. (2008), and in references cited therein.

A stronger heating of heavy ions can be understood from Eq. (23) and after expressing the effective temperature in terms of the ion mass  $T_{eff}(m_i) = m_i v_{max}^2 / (3\kappa)$ . From the derivative  $dT_{eff}(m_i) / dm_i > 0$ , we find that the heating increases with the ion mass if:

$$k_y^4 \rho_i^4 \left( \frac{e\phi}{\kappa T_i} \right)^2 > 1.9. \quad (25)$$

For  $\lambda_y = 0.5$  m,  $\lambda_z = 10$  km,  $L_n = 100$  m, we obtain from Eq. (18)  $\omega_i / \omega_r = 0.26$  and  $\omega_r = 254$  Hz. Note that in this case  $a \simeq 1$  and the stochastic heating is in action. Assuming small starting perturbations  $e\phi / (\kappa T_i) = 0.01$ , i.e.,  $\phi = 0.86$  V, the value  $\phi = 60$  V is achieved within  $\tau_g = 0.06$  s. Those were the reasons for the amplitudes of  $\phi$  used in the preceding section.

For  $\phi = 60$  V we then have  $T_i(\lambda_y, \mu) = 0.881 + 0.057\mu / \lambda_y^2 + 1.78\lambda_y^2 / \mu$  (normalized to the starting temperature  $T_i = 10^6$  K). In Fig. 8, we plot the obtained temperature in terms of the ion mass (normalized to the proton mass), and the perpendicular wavelength  $\lambda_y$ . It is seen that for short  $\lambda_y$ , and therefore for fast growing modes, *the heating is always larger for heavier ions*.

Using the same starting set of parameter values as above, by using Eqs. (22) and (23), in Table 1 we calculated the effective increase of the ion temperature for hydrogen

and helium for several wave amplitudes and perpendicular wavelengths. The results confirm and quantify the conclusions drawn above. The stronger heating for helium (values in brackets) in the short wavelength range is because the condition (25) is easily satisfied. Obviously, the proposed mechanism is more than efficient enough to heat the ions in the solar corona to the observed temperatures.

Assuming again small perturbations  $e\phi/(\kappa T_i) = 0.01$  for  $\lambda = 0.5$  m,  $L_n = 100$  m we have the above given values for  $\omega_i, \omega_r$ , and the value  $\phi = 60$  V achieved within  $\tau_g = 0.06$  s. The maximum energy released per unit volume is  $\Sigma_{max} = n_0 m_i v_{max}^2 / 2 = 0.04$  J/m<sup>3</sup>. The energy release rate  $\Gamma_{max} = \Sigma_{max} / \tau_g \simeq 0.7$  J/(m<sup>3</sup> s) amounts to 4 orders of magnitude above the necessary value.

However, for  $L_n = 100$  km (i.e., setting  $s = 1000$ ) we obtain  $\omega_i = 0.07$  Hz,  $\omega_r = 0.25$  Hz,  $\tau_g = 64$  s, and consequently  $\Gamma_{max} = 6.3 \cdot 10^{-4}$  J/(m<sup>3</sup> s), that is around 10 times the value presently accepted as necessary. Hence, the heating rate in large magnetic loops comes close to the required values. Similar estimates may be made for still larger  $L_n$ , yet the conditions under which the previous expressions are derived become violated and a numerical approach is required in this case.

For the typically achieved effective temperatures from Table 1, we have a heating rate of ions of the order of  $10^7 - 10^8$  K/s, which is similar to the heating rate obtained in the experiments Sanders et al. (1998); McChesney et al. (1987). Observe also that the magnitude of the electric field which we are dealing with, is of the same order as in the experiments.

However, some effects that are not included here may reduce the energy yield, especially at shorter spatial scales. They read as follows. In reality, the nonlinearity Lee & Okuda (1976) and collisions lead to the radial flattening of the density profile in the region occupied by the wave, resulting in the saturation of the growth. The flattening in some region  $\Delta r$  occupied by the wave, around a point  $r_0$ , leads to the saturation of the instability in this particular region. However, the process is accompanied by a simultaneous steepening of the density profile outside the region  $r_0 \pm \Delta r/2$ . These newly created (and also even steeper) density gradients will support the excitation of new modes now at different positions in radial direction. So here we have a sort of 'double cascade': the regions affected by the excitation of waves (and the heating) are shifting radially in both positive and negative directions. In other words, the starting instability (and heating) initiated around the position  $r_0$  (and in the same time extraordinarily elongated in the axial direction because  $k_z/k_y \ll 1$ ) will have the tendency of spreading radially.

The energy diffusion (due to any reason) in the perpendicular direction may reduce the local effects of the demonstrated strong heating rate. The earlier given Eq. (19) describes the coupling with the Alfvén wave, that is proportional to  $k_z k_y$ . All these effects (the nonlinearity, collisions, particle acceleration by the electric field, diffusion, and coupling with the Alfvén wave) will more effectively act on short scales. All of them, except the particle acceleration, will tend to reduce the mode amplitude. The actual values for  $\Gamma$  are thus expected to be below  $\Gamma_{max}$ . Therefore, the apparently too large release of energy at short scales, as formally obtained above, may in reality be considerably re-

duced. Clearly, more accurate estimates and more detailed description may be obtained only numerically.

Some additional features of the drift wave may also play a crucial role. First, the mode becomes easily nonlinear, and, second, within the nonlinear theory it allows a double cascade in  $\vec{k}$ -space, i.e., the transport of the wave energy both towards large and short wavelengths. Hence, due to nonlinear three-wave parametric interaction, a mode growing for certain  $\omega_0, \vec{k}_0$  will tend to excite modes at rather different (both smaller and larger)  $\omega_j, \vec{k}_j$ , and in the end those will always include the modes that heat the system most effectively. For example, the shape of Eq. (23) reveals that  $v_{max} \sim a_1 k_y + a_2 / k_y$  and, in terms of  $k_y$ ,  $v_{max}$  has a minimum at  $k_c^2 = 1.9 \kappa T_i / (\rho_i^2 e \phi)$ . Hence, even if a mode with wave number  $k_c$  does not produce a so large maximum bulk velocity  $v_{max}$ , it will nonlinearly excite modes with  $k_y$  far from  $k_c$  and there will be a stronger heating with this nonlinearly generated mode.

### 4.3 Heating of cool corona

In sections 4.1 and 4.2, we have demonstrated the possibility for sustainable coronal temperatures of around million K with the discussed drift wave mechanism. Assume now a relatively cool starting corona, with a temperature of only  $10^4$  K (the value taken high enough in order to neglect the presence of neutrals) and let us calculate the time that is needed to achieve the temperature of 1 million K, using the same mechanism.

We first chose the least favorable value  $k_y = k_c$  calculated above. This yields  $a = 1.9$  for any mode amplitude  $\phi$ , so we have the stochastic heating in action. For these  $a, k_c$ , from Eq. (23) we obtain  $v_{max} = 3.8 \Omega_i \rho_i [e\phi / (1.9 \kappa T_i)]^{1/2}$ . The effective temperature of 1 million K implies that the mode amplitude has the value  $\phi = \phi_m = 34$  V. This then yields  $k_y = k_c = 23.14$  1/m and  $\lambda_c = 0.27$  m.

Hence, choosing  $\lambda = \lambda_c$ , and  $\lambda_z = 50$  km,  $L_n = 100$  m, and  $n_0 = 10^{15}$  m<sup>-3</sup>, from Eqs. (17) and (18) we find  $\omega_r = 18.3$  Hz and  $\gamma = 0.75$  Hz. Assuming a small starting perturbation of the potential  $\phi = 0.0086$  V, i.e.,  $e\phi/(\kappa T_i) = 0.01$ , with the given growth rate we find out that the mode amplitude  $\phi_m$  (at which the temperature achieves the required value of million K due to the stochastic heating), is reached at longest within 11 s. For any other value of  $\lambda_y$  we will have a shorter growing and heating time.

## 5 KINETIC CURRENT-DRIVEN DRIFT WAVE INSTABILITY

In the presence of an additional energy source, in the form of an electron current in the direction of the magnetic field vector, the drift wave becomes even more unstable as compared to the previous collisionless kinetic instability. The mode frequency and the growth rate, with some additional features and details (Hatakeyama et al. 1980), are then given by:

$$\omega_r = \omega_{*e} \frac{\Lambda_0(b_i)}{1 + [1 - \Lambda_0(b_i)]\eta_\perp} \left[ 1 + \frac{1 + [1 - \Lambda_0(b_i)]\eta_\perp + \Lambda_0(b_i)\eta_z}{1 + [1 - \Lambda_0(b_i)]\eta_\perp} \frac{k_z^2 v_{Tiz}^2}{2\omega_{*ep}^2} \right] \quad (26)$$

**Table 1.** Plasma heating for hydrogen and helium (in brackets) ions for several values of the perpendicular wavelength and the wave amplitude  $\phi$ . The maximum stochastic velocity is given by Eq. (23) and the effective temperature obtained by heating is  $mv_{max}^2/(3\kappa)$ .

$\phi = 60$ [V]		
$\lambda_y$ [m]	$v_{max}$ [m/s]	$T_{eff}$ [K]
0.3	$2.12 \cdot 10^5$ ( $1.50 \cdot 10^5$ )	$1.82 \cdot 10^6$ ( $3.50 \cdot 10^6$ )
0.5	$2.20 \cdot 10^5$ ( $1.10 \cdot 10^5$ )	$1.96 \cdot 10^6$ ( $2.01 \cdot 10^6$ )
0.8	$2.79 \cdot 10^5$ ( $1.78 \cdot 10^5$ )	$3.14 \cdot 10^6$ ( $1.78 \cdot 10^6$ )
$\phi = 80$ [V]		
$\lambda_y$ [m]	$v_{max}$ [m/s]	$T_{eff}$ [K]
0.3	$2.54 \cdot 10^5$ ( $1.89 \cdot 10^5$ )	$2.61 \cdot 10^6$ ( $5.78 \cdot 10^7$ )
0.5	$2.45 \cdot 10^5$ ( $1.37 \cdot 10^5$ )	$2.43 \cdot 10^6$ ( $3.02 \cdot 10^6$ )
0.8	$2.95 \cdot 10^5$ ( $1.21 \cdot 10^5$ )	$3.50 \cdot 10^6$ ( $2.35 \cdot 10^6$ )
$\phi = 100$ [V]		
$\lambda_y$ [m]	$v_{max}$ [m/s]	$T_{eff}$ [K]
0.3	$2.96 \cdot 10^5$ ( $2.30 \cdot 10^5$ )	$3.54 \cdot 10^6$ ( $8.62 \cdot 10^7$ )
0.5	$2.71 \cdot 10^5$ ( $1.62 \cdot 10^5$ )	$2.95 \cdot 10^6$ ( $4.23 \cdot 10^6$ )
0.8	$3.10 \cdot 10^5$ ( $1.36 \cdot 10^5$ )	$3.88 \cdot 10^6$ ( $3 \cdot 10^6$ )

$$\omega_i = \frac{\omega_r \pi^{1/2}}{1 + [1 - \Lambda_0(b_i)]\eta_{\perp}} \left[ 1 + \frac{\eta_z \Lambda_0 k_z^2 v_{Tiz}^2 / \omega_{*ep}^2}{2[1 + [1 - \Lambda_0(b_i)]\eta_{\perp}]} \right] \times \left\{ \frac{u_0}{v_{Te}} + \frac{\omega_{*e} - \omega_{*ep}}{k_z v_{Te}} - \Lambda_0(b_i) \frac{\eta_z \omega_{*ep} + \omega_{*e}}{k_z v_{Tiz}} \right\} \times \exp[-\omega_{*ep}^2 / (k_z^2 v_{Tiz}^2)]. \quad (27)$$

Here,  $u_0$  is the electron current, the starting ion temperatures in the perpendicular and parallel direction are allowed to be different, and we use the notation from Hatakeyama et al. (1980)  $\eta_{\perp,z} = T_e/T_{i,\perp,z}$ ,  $v_{Tiz}^2 = \kappa T_{iz}/m_i$ , and  $\omega_{*ep} = \omega_{*e} \Lambda_0(b_i) / [1 + (1 - \Lambda_0(b_i))\eta_{\perp}]$ .

In solar corona environment, such electron currents may appear in the processes of magnetic reconnection. An example with the same phenomenon for the terrestrial atmosphere is given in Serizawa & Sato (1984).

We calculate the growth rate (27) numerically by taking  $B_0 = 10^{-3}$  T,  $n_0 = 10^{13}$  m $^{-3}$ ,  $L_n = [(dn_0/dx)/n_0]^{-1} = 1$  km,  $T_e = T_{i\perp} = 10^6 = 2T_{iz}$ , and  $\lambda_z = 200$  km. This different set of parameters is chosen only for a change, in view of the comments given earlier in Sec. 4 (see also Fig. 6). The result is presented in Fig. 9, where the growth rate  $\omega_i(\lambda_y, u_0)$  is normalized to the wave frequency  $\omega_r(\lambda_y, u_0)$ . We observe that for the given set of parameters, the current additionally increases the growth rate. This is seen by comparing the limits  $u_0 = 0$  and  $u_0 = 10$ , for e.g.  $\lambda_y = 15$  m, where the growth rate is increased by about a factor 20. However, the effect is of less importance for shorter wavelength (see the limit  $\lambda_y = 5$  m). In the given example, the mode frequency is below  $\omega_{*e}$ , so that the wave is growing anyhow, and this is due to the kinetic effects presented in the previous sections.

The real importance of such an electron flow is completely different in the limit  $\omega \simeq \omega_{*e}$  when the instability sets in provided that the electron current exceeds a certain threshold. This may be checked for example by setting larger values for  $B_0$  when the kinetic instability from the previous

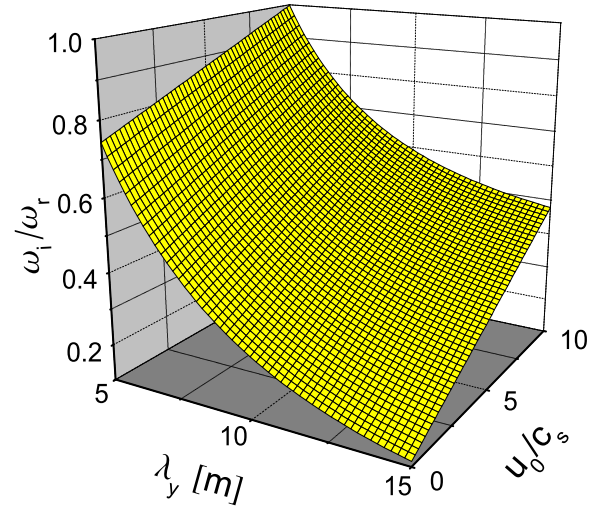


**Figure 9.** Growth rate  $\omega_i(\lambda_y, u_0)/\omega_r(\lambda_y, u_0)$  from Eqs. (26) and (27) for the kinetic + current-driven drift-wave instability in the case  $B_0 = 0.001$  T.

sections vanishes (because for the given parameters  $\omega_{*e}$  is reduced so that  $\omega \geq \omega_{*e}$ ). Yet, the wave instability reappears for a sufficiently large  $u_0$ , but it is now the current-driven one. Exactly such a sort of behavior was *verified experimentally* in Hatakeyama et al. (1980). Hence, for example we take the magnetic field for one order of magnitude larger  $B_0 = 10^{-2}$  T, and the result is presented in Fig. 10. The contour lines of  $\omega_i(\lambda_y, u_0)/\omega_r(\lambda_y, u_0)$  in Fig. 10 yield only the current-driven drift wave for sufficiently large  $\lambda_y$ .

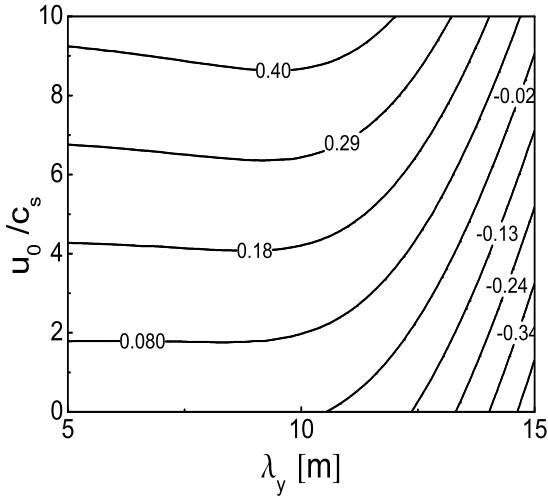


**Figure 10.** Contour lines of  $\omega_i(\lambda_y, u_0)/\omega(\lambda_y, u_0)$  from Eqs. (26) and (27) for  $B_0 = 0.01$  T, showing the current-driven drift-wave instability in the vicinity of threshold.

### 5.1 Plasma heating

The heating of the plasma by this current-driven drift-wave instability, as *experimentally measured* in Hatakeyama et al. (1980), has similar properties as the one discussed in the previous text. This implies the following facts: i) the anisotropy in the ion heating ( $T_{i\perp} > T_{iz}$ , ii) the heating time being comparable to the growth time of the drift wave and proportional to the wave energy (square amplitude), iii) the perpendicular heating being associated with the leading order perturbed perpendicular drift, while the parallel heating is associated with the ion Landau damping.

We stress that the *collisional* counterpart of the above described current-driven drift-wave instability, applicable to the lower solar atmosphere, may be found in Ellis & Motley (1978) where it has been explained and *also experimentally verified*.

## 6 ION-CYCLOTRON DRIFT WAVE

In the case of high-frequency electrostatic perturbations satisfying the condition  $\omega_r \sim \Omega_i$ , and in the presence of a density gradient, we have an ion-cyclotron drift (ICD) wave, also called the ion Bernstein mode in the literature (Ichimaru 1980). This mode has been theoretically predicted (Mikhailovskii & Timofeev 1963) and experimentally verified (Hendel & Yamada 1974) long ago. The kinetic description given in Ichimaru (1980); Mikhailovskii & Timofeev (1963); Hendel & Yamada (1974) reveals the same instability mechanism as in the case of the kinetic drift wave instability presented before. However, in order for the instability to take place, the drift-wave branch and the ion-cyclotron branch must get close to each other. In that case, instead of the intersection of two dispersion lines, we have only one complex-conjugate solution. Clearly, to have this, the equilibrium density scale length must be very short to make the frequency of the drift part high, this because for the drift wave  $\omega_r \sim 1/L_n$ . An application to solar plasma of this in-

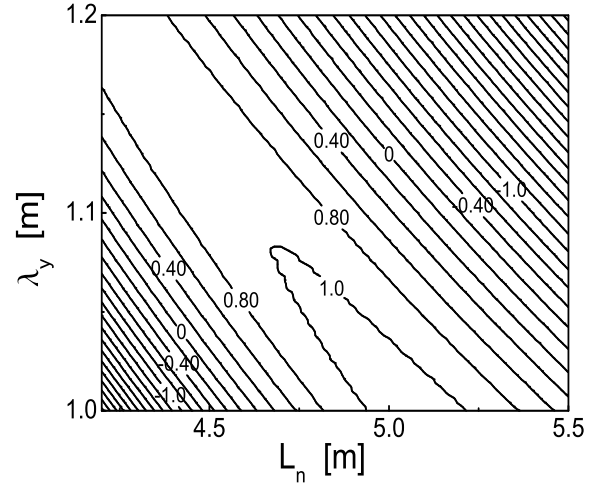


**Figure 11.** Contour plot of  $S(k_y, L_n)$  from Eq. (28). The ICD mode is growing for  $S(k_y, L_n) > 0$ .

stability is discussed in Vranjes & Poedts (2008a). As shown in Ichimaru (1980), the ICD mode grows if the following instability condition is satisfied:

$$S(k_y, L_n) = 2k_y^2 \lambda_d^2 \omega_1 (\omega_1 + \omega_2) \delta - (\omega_1 - \omega_2)^2 (1 + k_y^2 \lambda_d^2 - 2\delta) > 0. \quad (28)$$

Here,  $\omega_1 = \omega_{*e}/(1 + k_y^2 \lambda_d^2)$ ,  $\omega_2 = \Omega_i [1 + \delta/(1 + k_y^2 \lambda_d^2)]$ ,  $\lambda_d^2 = \rho_i^2 m_e/m_i + \lambda_{de}^2 T_i/T_e$ ,  $\lambda_{de} = v_{Te}/\omega_{pe}$ ,  $\delta = 1/[(2\pi)^{1/2} k_y \rho_i]$

We stress that the ion-cyclotron mode itself has been discussed a lot in the past in the context of problems related to the heating of the solar corona, see e.g. Cranmer et al. (1999), Cranmer (2000), Hollweg & Isenberg (2002). The reasons for this are the same as those discussed in the previous sections: the evidence obtained from in situ measurements in the solar wind and coronal holes of resonant ion cyclotron heating, and a preferential heating of coronal ions (with respect to electrons), that in the same time is most dominant in the direction perpendicular to the magnetic field lines. In this context, *the damping* of such IC waves is believed to be a good candidate for the consequent coronal heating and solar wind acceleration (Markovskii 2001). Yet, as in many wave-heating scenarios of the corona proposed in the past, there is the problem of the source for the required generation of such IC waves throughout the corona. The effects proposed as sources for the IC mode are global resonant MHD modes (Markovskii 2001), currents (Forslund 2001; Toichi 1971), etc. However, as a rule, these effects themselves need some source, so the problem is not solved but merely shifted to another problem.

The analysis performed in Vranjes & Poedts (2008a) and in the previous sections, demonstrates that such a source (the density gradient) exists, and the mechanism which it implies is well known in the literature but not used or studied in the context of the solar plasma, and it is able to produce growing ICD modes on massive scales. For example, in Fig. 9 we give the contour plot of  $S(k_y, L_n)$  from Eq. (28). The figure shows a narrow range of  $L_n$  and  $\lambda_y$  within which the ICD is growing,  $S(k_y, L_n) > 0$ . The parameters are the same as before:  $B_0 = 10^{-3}$  T,  $n_0 = 10^{13}$  m $^{-3}$ , and

$T_e = T_i = 10^6$  K. The instability shown here implies short-scale density inhomogeneities. However, this scale can be increased for example by decreasing the magnetic field intensity. Setting  $10^{-4}$  T and also reducing the number density by one order of magnitude, yields the necessary density scale length  $L_n$  for the unstable modes of the order of 60 meters. Observe that such reduced values may be obtained e.g. by moving further along a flux tube, implying that the mechanism may work at various altitudes in the solar atmosphere.

### 6.1 Stochastic heating of plasma by ICD wave

A *stochastic* heating mechanism, similar to the case discussed previously for the drift wave, is also known to exist in this particular frequency domain. This has been discussed in Karney & Bers (1977). It is shown that the stochastic heating by a perpendicularly propagating electrostatic wave, satisfying the condition  $\omega_r \simeq l\Omega_i$ ,  $l = 1, 2, \dots$ , takes place if the mode amplitude exceeds the limit:

$$E > \frac{B_0}{4} \frac{\omega_r}{k_\perp} \left( \frac{\Omega_i}{\omega_r} \right)^{1/3}. \quad (29)$$

The condition is obtained after analyzing the same equations as Eq. (21). This yields the wave potential  $\phi = B_0 \Omega_i l^{2/3} / 4 = 24l^{2/3}$ . The results from Vranjes & Poedts (2008a) provide the maximum mode growth rate  $\omega_i/\omega_r \simeq 0.1$ . For the given magnetic field we have  $\Omega_i \simeq 10^5$  Hz for protons. Now, assuming small starting electrostatic perturbations  $e\phi/(\kappa T_i) \simeq 0.01$ , and setting  $l = 1$ , we find out that the required wave potential amplitude is achieved within about  $3 \cdot 10^{-4}$  s only! Hence, in the given coronal environment the stochastic heating condition (29) is practically instantaneous. It develops in the way already described in the pervious text.

## 7 CONCLUDING COMMENTS

We have presented a few (out of many) physical effects that make the drift mode growing. There exist many more phenomena that lead to the growth of drift waves but these are not discussed here at all, e.g. the temperature gradient driven drift wave instability, shear flow instability, etc. As a matter of fact, the presence of a temperature gradient implies an additional source of energy and an instability provided that the temperature and density gradients have opposite sign (Rudakov & Sagdeev 1961), i.e.,  $\partial \ln T / \partial \ln n_0 < 0$ . One particularly strong mechanism leading to an instability is a sheared flow. The term ‘shear flow’ refers to the flow of the plasma as a whole along the magnetic field vector and having in the same time a gradient in the perpendicular direction. Such a current-less instability [known also as D’Angelo mode (D’Angelo 1965)] has an extra energy source in the flow gradient. A kinetic theory analysis of this instability as given in Ganguli et al. (1994), while its most recent *experimental verification* may be found in Kaneko et al. (2003). In Saleem et al. (2007) such a shear flow instability is discussed within the fluid theory in application to coronal spicules, showing strongly growing modes with the possibility for  $\omega_i > \omega_r$ . Because of the radial density gradients, solar spicules are an ideal

nursery for the drift wave instability. Growing drift waves are simply carried upwards by the plasma flow inside each of them. In the same time they are numerous (at least  $10^5$  of them are present throughout the Sun at every moment). There are also evidences of the presence of plasma flows along the magnetic flux loops Schrijver et al. (1999). While the magnitude of these axial flows is determined (showing subsonic flows with velocities up to 100 km/s), their eventual inhomogeneity in the radial direction remains an open question. Yet, there are no obvious physical reasons that would exclude them. The inflow of more dense plasma along a magnetic flux tube from lower (cooler) layers may then imply the simultaneous presence of a density gradient (towards the axis) and a temperature gradient (outward oriented). In such a geometry, the mentioned temperature-gradient instability may develop, or/and it may be combined with the shear-flow instability.

In reality, and in particular in the heating processes in the solar corona, the simple growth-damping process of a coherent wave, and the consequent heating due to the resonant interaction with plasma particles, can not be a completely accurate picture. It is rather an interplay between various processes that may happen in the same time and place, like collisions, mode growth, kinetic effects, nonlinearity and turbulence, and stochastic ion and electron heating. The results presented here show that the stochastic heating related to the drift wave is a powerful mechanism that switches on for sufficiently large mode amplitudes. The properties of the resulting heating process are such that they are consistent with all the observed features of the plasma heating in the solar atmosphere. On the other hand, there is plenty of energy for the mode itself, stored in the omnipresent density gradients. To our knowledge, there is no other available heating model like the one presented in this work, that is so clearly able to fulfill all these requirements.

The presented mechanism removes the necessity for explaining the most crucial problems of coronal heating: namely i) how the (right amount of) energy is transmitted from ‘sources below’ the photosphere to the corona, and ii) how this energy is dissipated locally in the corona (at the right rate). Instead, we showed, first, that a sufficient amount of energy for driving drift modes is already present in the corona, and, second, that it is naturally transmitted to the different plasma species by well known effects that are, however, beyond the standardly used models and theories. Hence, the proposed mechanism is based on a novel paradigm that allows a self-consistent solution model. The heating mechanism implies instabilities on time and spatial scales that are currently not directly observable by space probes. However, all the effects presented here are directly experimentally verified under laboratory conditions. Their indirect confirmation in the context of the solar corona seems to be also beyond doubts. This is because the *consequences* of the heating process, as enlisted earlier in the text (temperature anisotropy, better heating of heavier ions, hotter ions than electrons), are indeed verified by satellite observations.

## ACKNOWLEDGMENTS

The results presented here are obtained in the framework of the projects G.0304.07 (FWO-Vlaanderen), C 90347

(Prodex), GOA/2009-009 (K.U.Leuven). Financial support by the European Commission through the SOLAIRE Network (MTRN-CT-2006-035484) is gratefully acknowledged. TRACE (Fig. 1) is a mission of the Stanford-Lockheed Institute for Space Research, and part of the NASA Small Explorer program.

## REFERENCES

- Aschwanden, M. J., 2001, *ApJ*, 560, 1035  
 Aschwanden, M. J., 2004, *Physics of the Solar Corona*. Springer-Verlag, Belin-Heidelberg-New York  
 Aschwanden, M. J., Wülser, J. P., Nitta, N. V., Lemen, R. R., 2008a, *ApJ*, 679, 827  
 Aschwanden, M. J., Lee, J. K., Gary, G. A., Smith, M., Inhester, B., 2008b, *Sol. Phys.*, 248, 359  
 Bittencourt, J. A., 1995, *Fundamentals of Plasma Physics*. Sao José dos Campos, Brazil  
 Brossier, P., Deschamps, P., Gravier, R., Pellat, R., Renaud, C., 1971, *Phys. Rev. Lett.*, 26, 124  
 Chen, F. F., 1988, *Introduction to Plasma Physics and Controlled Fusion*. Plenum Press, New York  
 Cranmer, S. R., Field, G. B., Kohl, J. L., 1999, *ApJ*, 518, 937  
 Cranmer, S. R., 2000, *ApJ*, 532, 1197  
 Cranmer, S. R., Panasyuk, A. V., Kohl, J. L., 2008, *ApJ*, 678, 1480  
 Cuseri, I., Mullan, D., Poletto, G., 1999, *Space Sci. Rev.*, 87, 153  
 D'Angelo, N., 1965, *Phys. Fluids*, 8, 1748  
 D'Angelo, N., 1968, *ApJ*, 154, 401  
 De Pontieu, B., McIntosh, S. W., Carlsson, M., Hansteen, V. H., Tarbell, T. D., Schrijver, C. J., Title, A. M., Shine, R. A., Tsuneta, S., Katsukawa, Y., Ichimoto, K., Suematsu, Y., Shimizu, T., Nagata, S., 2007, *Science*, 318, 1574  
 Dreicer, H., 1959, *Phys. Rev.*, 115, 238  
 Ellis, R. F., Motley, R. W., 1978, *Phys. Fluids*, 17, 582  
 Fletcher, L., Hudson, H. S., 2008, *ApJ*, 675, 1645  
 Forslund, D. W., 1970, *J. Geophys. Res.*, 75, 17  
 Ganguli, G., Keskinen, M. J., Romero, H., Heelis, R., Moore, T., Pollock, C., 1994, *J. Geophys. Res.*, 99, 8873  
 Hansteen, V. N., Leer, E., Holtzer, T. E., 1997, *ApJ*, 482, 498  
 Hasegawa, A., 1975, *Plasma Instabilities and Nonlinear Effects*. Springer-Verlag, Berlin Heidelberg  
 Hatakeyama, R., Oertl, M., Märk, E., Schrittwieser, R., 1980, *Phys. Fluids*, 23, 1774  
 Hendel, H. W., Yamada, M., 1974, *Phys. Rev. Lett.*, 33, 1076  
 Hollweg, J. V., Isenberg, P. A., 2002, *J. Geophys. Res.*, 107, 10.1029  
 Ichimaru, S., 1980, *Basic Principles of Plasma Physics*. The Benjamin/Cummings Publish. Comp., Reading, Massachusetts  
 Kadomtsev, B. B., 1965, *Plasma Turbulence*. Academic Press, London  
 Kaneko, T., Tsunoyama, T., Hatakeyama, R., 2003, *Phys. Rev. Lett.*, 90, 125001  
 Karney, C. F. F., Bers, A., 1977, *Phys. Rev. Lett.*, 39, 550  
 Karovska, M., Habbal, S. R., 1991, *ApJ*, 371, 402  
 Klimtchuk, J. A., 2006, *Solar Phys.*, 234, 41  
 Lee, W. W., Okuda, H., 1976, *Phys. Rev. Lett.*, 36, 870  
 Li, X., Habbal, S. R., Kohl, J. L., Noci, G., 1998, *ApJ*, 501, L133  
 Markovskii, S. A., 2001, *ApJ*, 557, 337  
 McChesney, J. M., Stern, R. A., Bellan, P. M., 1987, *Phys. Rev. Lett.*, 59, 1436  
 Mecheri, R., Marsch, E., 2008, *A&A*, 481, 853  
 Mikhailovskii, A. B., Timofeev, A. V., 1963, *Sov. Phys. JETP*, 17, 626  
 Milligan, R. O., Gallagher, P. T., Mathioudakis, M., Keenan, F. P., Bloomfield, D. S., 2005, *MNRAS*, 363, 259  
 Narain, U., Ulmschneider, P., 1990, *Space Sci. Rev.*, 54, 377  
 Nishida, Y., Ishii, K., 1974, *Phys. Rev. Lett.*, 33, 352  
 November, L. J., Koutchmy, S., 1977, *ApJ*, 466, 512  
 Pandey, B. P., Wardle, M., 2008, *MNRAS*, 385, 2269  
 Panofsky, W. K. H., Phillips, M., 1978, *Classical Electricity and Magnetism*. Addison-Wesley, Reading  
 Régnier, S., Parnell, C. E., Haynes, A. L., 2008, *A&A*, 484, L47  
 Revathy, P., 1977, *Sol. Phys.*, 53, 445  
 Rudakov, L. I., Sagdeev, R. Z., 1961, *Sov. Phys. Doklady*, 6, 415  
 Sanders, S. J., Bellan, P. M., Stern, R. A., 1998, *Phys. Plasmas*, 5, 716  
 Saleem, H., Vranjes, J., Poedts, S., 2007, *A&A*, 471, 289  
 Schrijver, C. J., Title, A. M., Berger, T. E., Fletcher, L., Hurlburt, N. E., Nightingale, R. W., Shine, R. A., Tarbell, T. D., Wolfson, J., Golub, L., Bookbinder, J. A., Deluca, E. E., McMullen, R. A., Warren, H. P., Kankelborg, C. C., Handy, B. N., De Pontieu, B., 1999, *Sol. Phys.*, 187, 261  
 Serizawa, Y., Sato, T., 1984, *Geophys. Res. Lett.*, 11, 595  
 Suzuki, T. K., 2004, *MNRAS*, 349, 1227  
 Toichi, T., 1971, *Sol. Phys.*, 18, 150  
 Vranjes, J., Poedts, S., 2004, *Phys. Plasmas*, 11, 891  
 Vranjes, J., Poedts, S., 2006, *A&A*, 458, 635  
 Vranjes, J., Poedts, S., 2006, *Phys. Plasmas*, 13, 122103  
 Vranjes, J., Poedts, S., 2007, *Phys. Plasmas* 14, 112106  
 Vranjes, J., Pandey, B. P., Poedts, S., 2007, *Phys. Rev. Lett.*, 98, 049501  
 Vranjes, J., Poedts, S., 2008a, *A&A*, 482, 653  
 Vranjes, J., Poedts, S., 2008b, *Phys. Plasmas*, 15, 034504  
 Vranjes, J., Poedts, S., Pandey, B. P., De Pontieu, B., 2008a, *A&A*, 478, 553  
 Vranjes, J., Kono, M., Poedts, S., Tanaka, M. Y., 2008b, *Phys. Plasmas*, 15, 092107  
 Vranjes, J., Poedts, S., 2009, *Phys. Plasmas*, 16, 022101  
 Warren, H. P., Ugarte-Urra, I., Doschek, G. A., Brooks, D. H., Williams, D. R., 2008, *ApJ*, 686, L131  
 Weiland, J., 2000, *Collective Modes in Inhomogeneous Plasmas*. Institute of Physics Pub., Bristol  
 Woo, R., Habbal, S. R., 1997, *ApJ*, 474, L139  
 Woo, R., 1996, *Nature*, 379, 321

This paper has been typeset from a  $\text{\TeX}$ / $\text{\LaTeX}$  file prepared by the author.

